ELECTRONIC SUPPORTING INFORMATION

Structure-Property Relationships Describing the Buried Interface Between Silicon Oxide Overlayers and Electrocatalytic Platinum Thin Films

Marissa E.S. Beatty,[†] Han Chen,[†] Natalie Y. Labrador, Brice J. Lee, Daniel V. Esposito*

Department of Chemical Engineering,
Columbia Electrochemical Energy Center,
Lenfest Center for Sustainable Energy,
Columbia University in the City of New York
500 W. 120th St., New York, NY 10027

[†]both authors contributed equally
*de2300@columbia.edu

Table of Contents

I. Atomic force microscopy (AFM) characterization of SiO_x|Pt electrodes

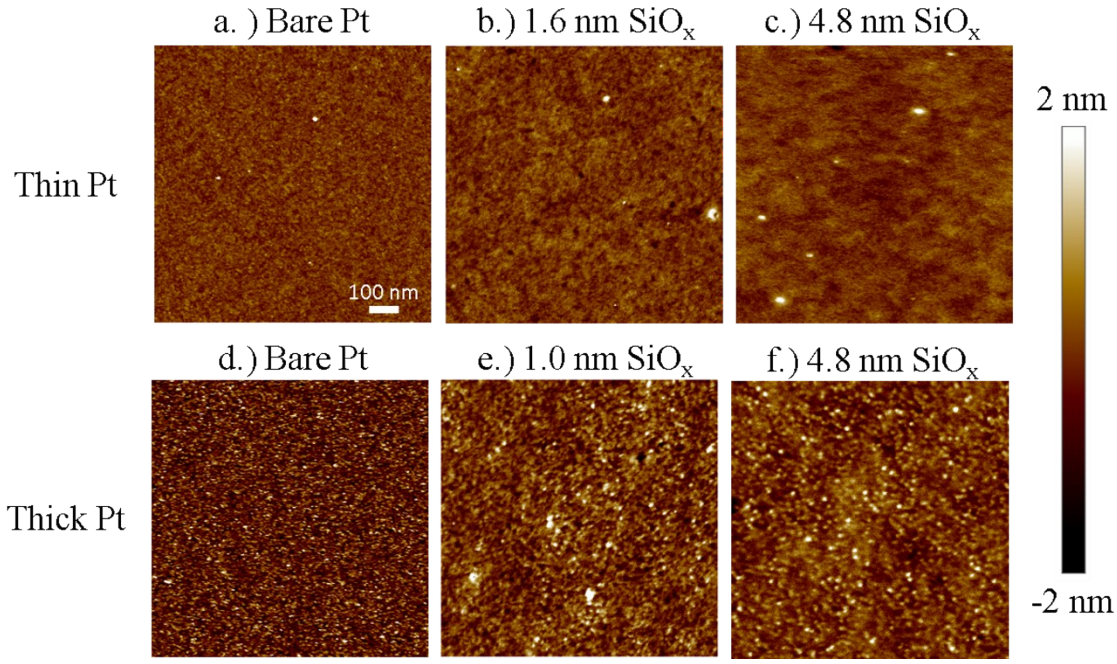

Figure S1. Representative AFM images of as-made 0 nm, 1.6 nm, and 4.8 nm SiO_x overlayers deposited on thin (3/2 nm) Pt/Ti thin film, and 0 nm, 1.0 nm, and 4.8 nm SiO_x overlayers deposited on thick (50 nm) Pt film. Pt and Ti layers were deposited sequentially by e-beam evaporation onto a $p^+Si(100)$ substrate.

II. X-ray photoelectron spectroscopy (XPS) characterization

2.1 Description of XPS fitting procedures

XPS measurements were made with a Phi XPS system at pressures < $2x10^{-10}$ Torr using a monochromatic Al Kα source (15 kV, 20 mA). Survey scans were first performed utilizing a charge neutralizer over the range of 0 to 1000 eV. Multiplex scans over regions of interest were then performed in sequence, with multiple scans of the same region being averaged for the presented figures. Raw data was exported to and processed using XPSPEAK 4.1 software.

The background signal of all raw spectra were fit with a Shirley model, and all peaks were fit using Lorentzian-Gaussian peak shapes. Peak center locations for the Pt $4f_{7/2}$ and Pt $4f_{5/2}$ peaks for metallic platinum were defined by characterizing a bare Pt electrode, where measurements were compared to values presented in literature,[1] and found to be in agreement. These values were used to define the metallic Pt $4f_{7/2}$ and Pt $4f_{5/2}$ peak center locations as 71.2 eV and 74.5 eV for all samples. Ratios between the fitted Pt $4f_{5/2}$ to Pt $4f_{7/2}$ peaks were confirmed to be 0.71, and all

subsequent fits were confined to this ratio. FWHM values between Pt $4f_{7/2}$ and Pt $4f_{5/2}$ peaks were set to be equivalent. All spectra for electrodes containing platinum oxide species (PtO_x) were fit with Pt 4f contributions of metallic Pt that were based on these parameters for as-made bare Pt. Additional peaks associated with the formation of PtO_x species were fit assuming the same multiplet splitting and Pt $4f_{5/2}$ to Pt $4f_{7/2}$ peak area ratios as metallic Pt, and followed the procedure of confining FWHM to be equivalent between associated doublet peaks, while leaving peak location and area as fitting parameters.

Asymmetry in peak shapes was determined by defining peak fitting parameters (TS=0.2 and TL=60) in the XPSPEAK software that gave the best fit for bare Pt control samples. Atomic concentrations were determined from the integrated peak areas of the primary photoemission peaks of each element (Pt 4f, O 1s, C 1s, Ti 2p) normalized to their respective atomic sensitivity factors (ASFs) available from literature.[2] The atomic concentration of element *i* was then calculated as the ratio of I_i/ASF_i divided by the sum of the ratios of (I_j/ASF_j) for all *j* elements. In calculating the concentrations of carbon that are reported in the manuscript, signal from elements associated with the metal substrate was excluded from the analysis to give an indication of the amount of carbon on and in the SiO_x overlayer. C 1s contributions from adventitious carbonaceous adsorptions were *not* subtracted from the analysis, meaning that the reported atomic % C values overestimate the amount of carbon within the SiO_x overlayers.

Pt 4f difference curves for the UV-Ozone treated and SiO_x coated substrates were obtained by normalizing the maximum peak height of the Pt $4f_{7/2}$ peak, relative to the background, for each sample to the height of the untreated, bare Pt sample. The signal associated with bare Pt was then subtracted from each Pt 4f spectra, and the resultant difference signal associated with PtO_x species was fit with three different Pt 4f peaks for PtO_{ad}, PtO, and PtO_2 based on peak center binding energies from literature.[3]

2.2 Description of XPS overlayer calculations

SiO_x overlayer thicknesses were estimated based on the integrated Si 2p and Pt 4f signal intensities (peak areas) based on a commonly used 2-layer overlayer model that accounts for attenuation of signal from a substrate material (S, i.e. Pt) by a thin overlayer (O, i.e. SiO_2) for a uniform, planar sample: [2]

$$\frac{I_o/ASF_o}{I_s/ASF_s} = \frac{1 - \exp\left[-d/\lambda^{o}_{imfp}(E_o)\cos\theta\right]}{\exp\left[-d/\lambda^{o}_{imfp}(E_s)\cos\theta\right]} \quad \text{(S1)}$$

where I is the integrated signal intensity (peak area), ASF is the atomic sensitivity factor, λ^{o}_{imfp} is the inelastic mean free path of an electron of kinetic energy E through the overlayer, d is the overlayer thickness, and θ is the emission angle between the spectrometer and sample normal. For SiO_x, the ASF of the Si 2p signal was adjusted by multiplying the ASF of elemental Si by the ratio of the atomic densities of Si in SiO_2 ($\rho_{Si,SiO2}$) to Si in metallic Si ($\rho_{Si,Si}$). Values of $\lambda^{o}_{imfp}(E_O)$ and $\lambda^{o}_{imfp}(E_S)$ were obtained from the empirical universal curve describing the relationship between λ^{o}_{imfp} and E for solid materials, and range from 1.7 nm to 2.2 nm for all materials in the fabricated samples.[4] In the cases where the substrate or overlayer is comprised of multiple materials (i.e. Pt-PtO_x), values for IMFP and ASF were determined as an average, based on the atomic percent of the species detected for the given material. These averages are calculated based on the assumption that the source of all Ti 2p and Pt 4f signal is from the substrate, and all Si 2p signal originates from the overlayer. Knowing the intensities, emission angle, sensitivity factors, and inelastic mean free paths for both layers, Equation S1 can be simplified to solve for d:

$$d = \lambda^{o}_{imfp} \cdot \cos(\theta) \cdot \ln\left[1 + \frac{\left(\frac{I_o}{ASF_o}\right)}{\left(\frac{I_s}{ASF_s}\right)}\right] \quad \text{(S2)}$$

2.3 XPS characterization of as-made SiO_x|Pt electrodes

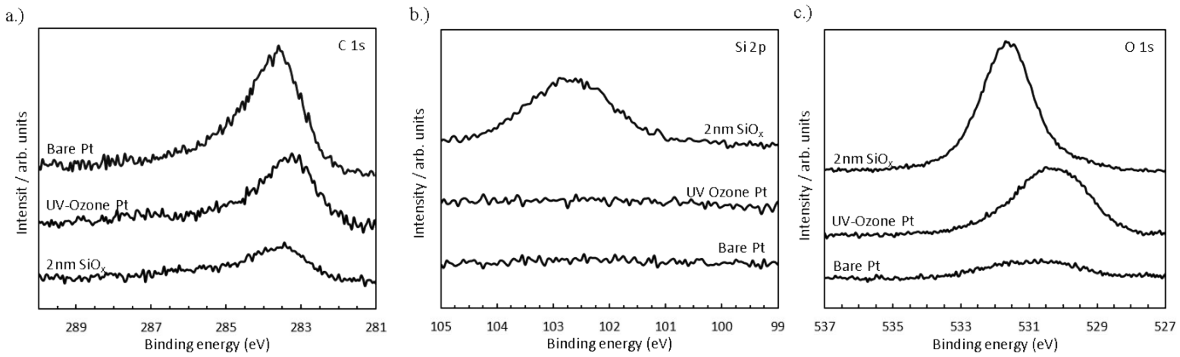

Figure S2. XPS Spectra of thick platinum substrates for bare platinum, platinum exposed to UV ozone treatment, and platinum with a continuous 1.9 nm silicon oxide overlayer. (a.) Comparison of Carbon 1s XPS spectra (b.) Comparison of Silicon 2p XPS spectra (c.) Comparison of Oxygen 1s XPS spectra.

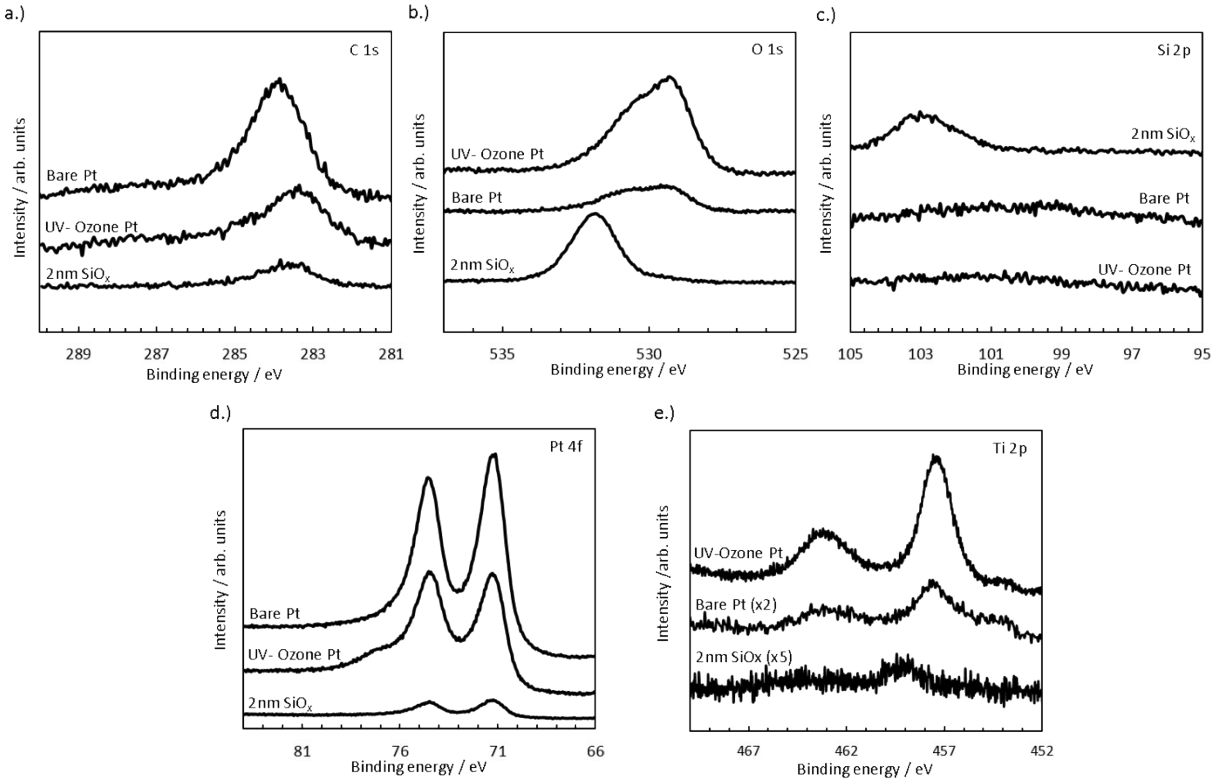

Figure S3. XPS Spectra of thin platinum substrates for bare platinum, platinum exposed to UV ozone treatment, and platinum with a continuous 2.1 nm silicon oxide overlayer. a.) Comparison of C 1s XPS spectra. b.) Comparison of O 1s XPS spectra. c.) Comparison of Silicon 2p XPS spectra. d.) Comparison of Platinum 4f XPS spectra. e.) Comparison of Ti 2p XPS spectra.

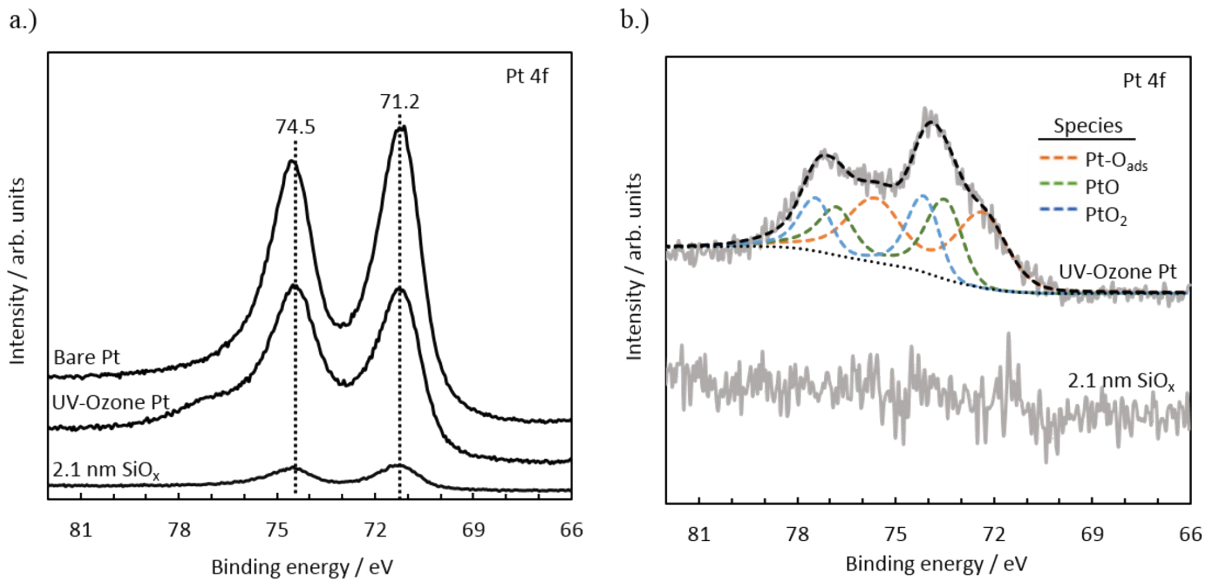

Figure S4. a.) XPS Pt 4f spectra of two unencapsulated Pt electrodes ("Bare Pt" and "UV ozone Pt") and a SiO_x|(thin Pt) electrode with t_{SiOx}=2.1 nm. The spectra were normalized to the maximum Pt 4f 7/2 peak intensities for all samples. b.) Pt 4f difference spectra (grey curves) were obtained by subtracting the spectrum of the untreated bare Pt electrode from those of the PtO_x-containing electrodes. The black dashed lines represent the fitted background and overall fitted spectra.

III. Cyclic voltammograms in sulfuric acid

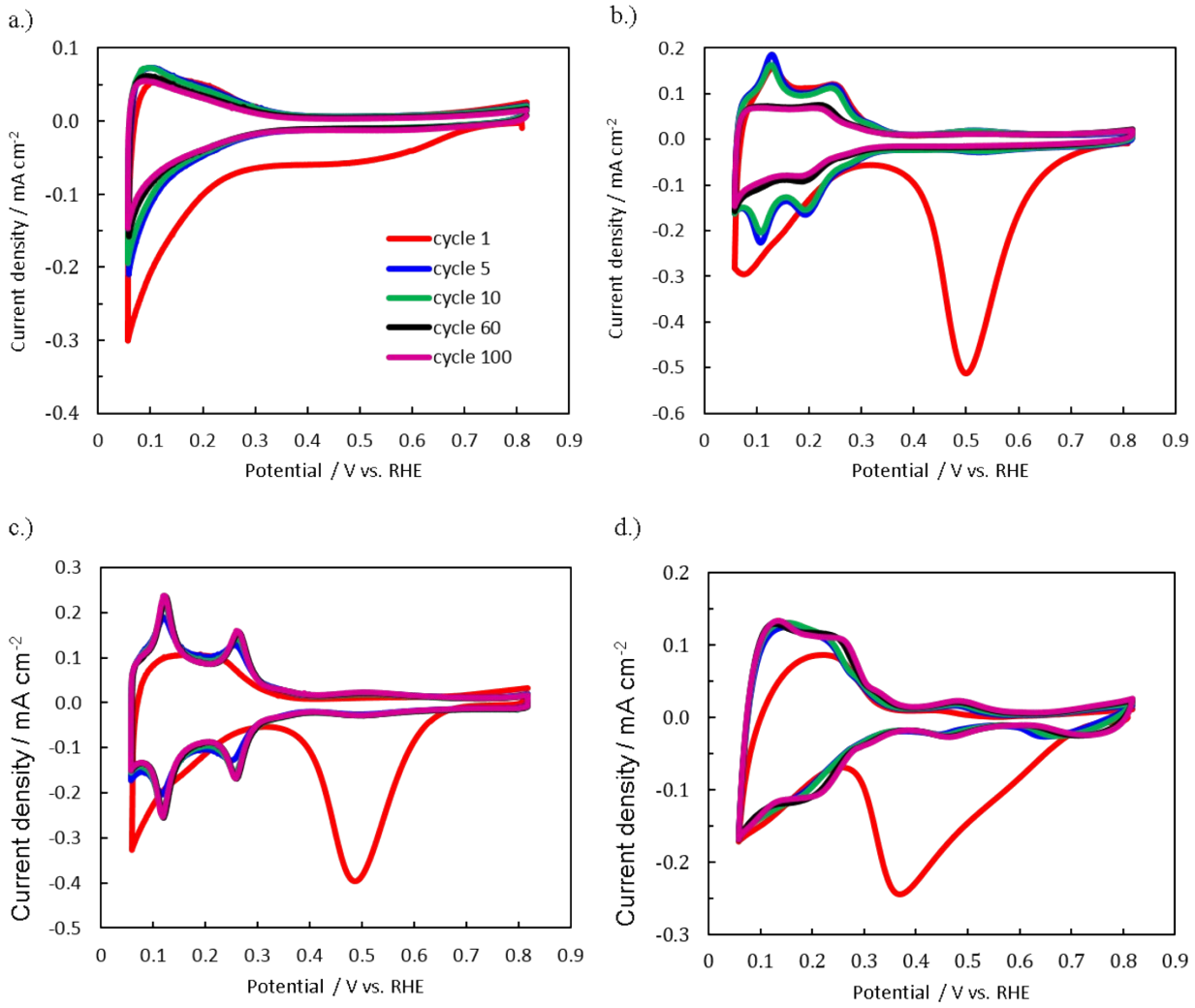

Figure S5. Narrow window CVs conducted at 100 mVs^{-1} over a range of 0.06 – 0.82 V vs. RHE in 0.5 M deaerated H_2SO_4 for SiO_x|(thick Pt) electrodes at varying cycle numbers for SiO_x thicknesses of a.) 0 nm b.) 1.4 nm c.) 4.6 nm and d.) 10.3 nm.

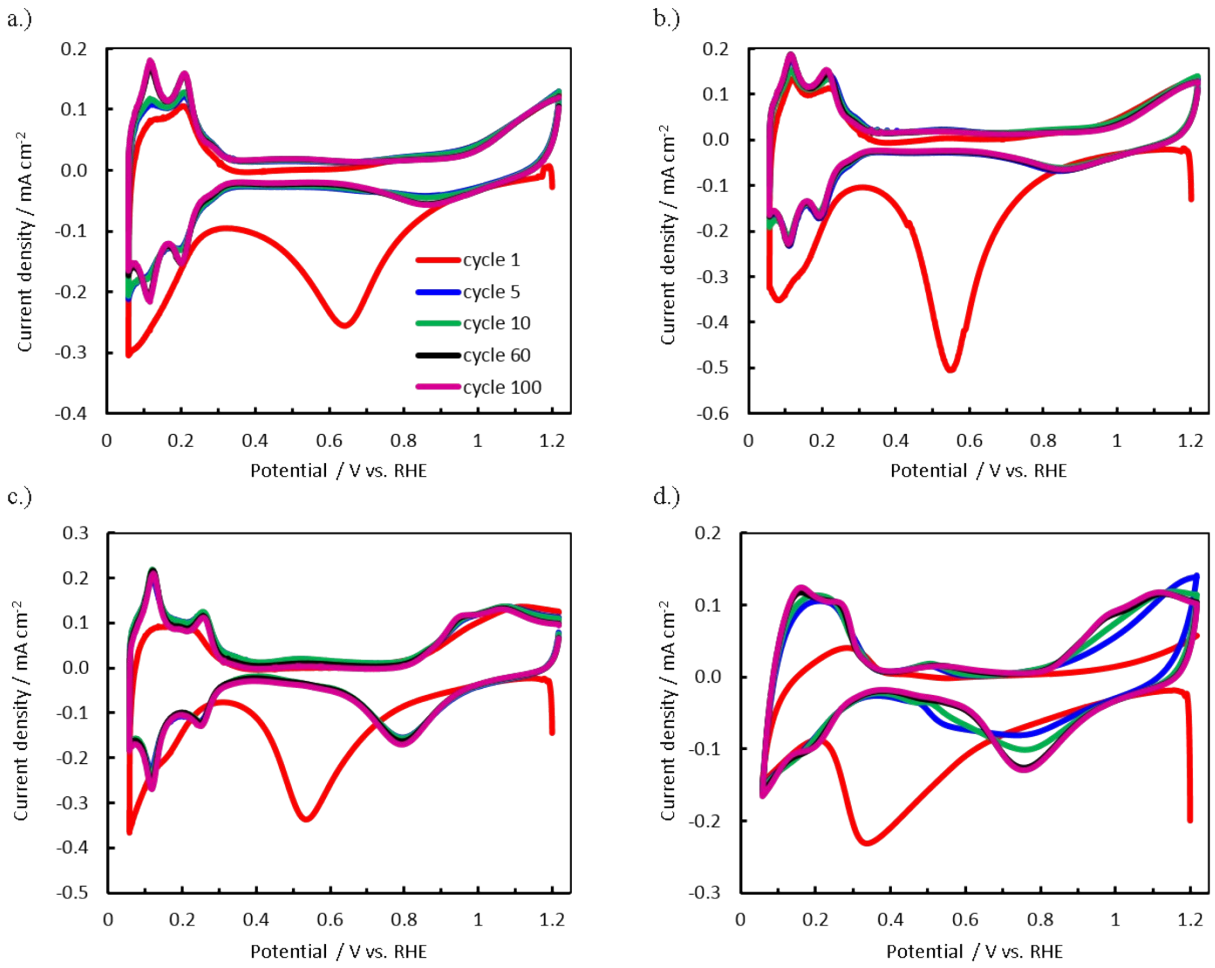

Figure S6. Wide window CVs conducted at 100 mVs^{-1} over a range of 0.06 – 1.22 V vs. RHE in 0.5 M deaerated H_2SO_4 for SiO_x|(thick Pt) electrodes at varying cycle numbers for SiO_x thicknesses of a.) 0 nm b.) 1.4 nm c.) 4.6 nm and d.) 10.3 nm.

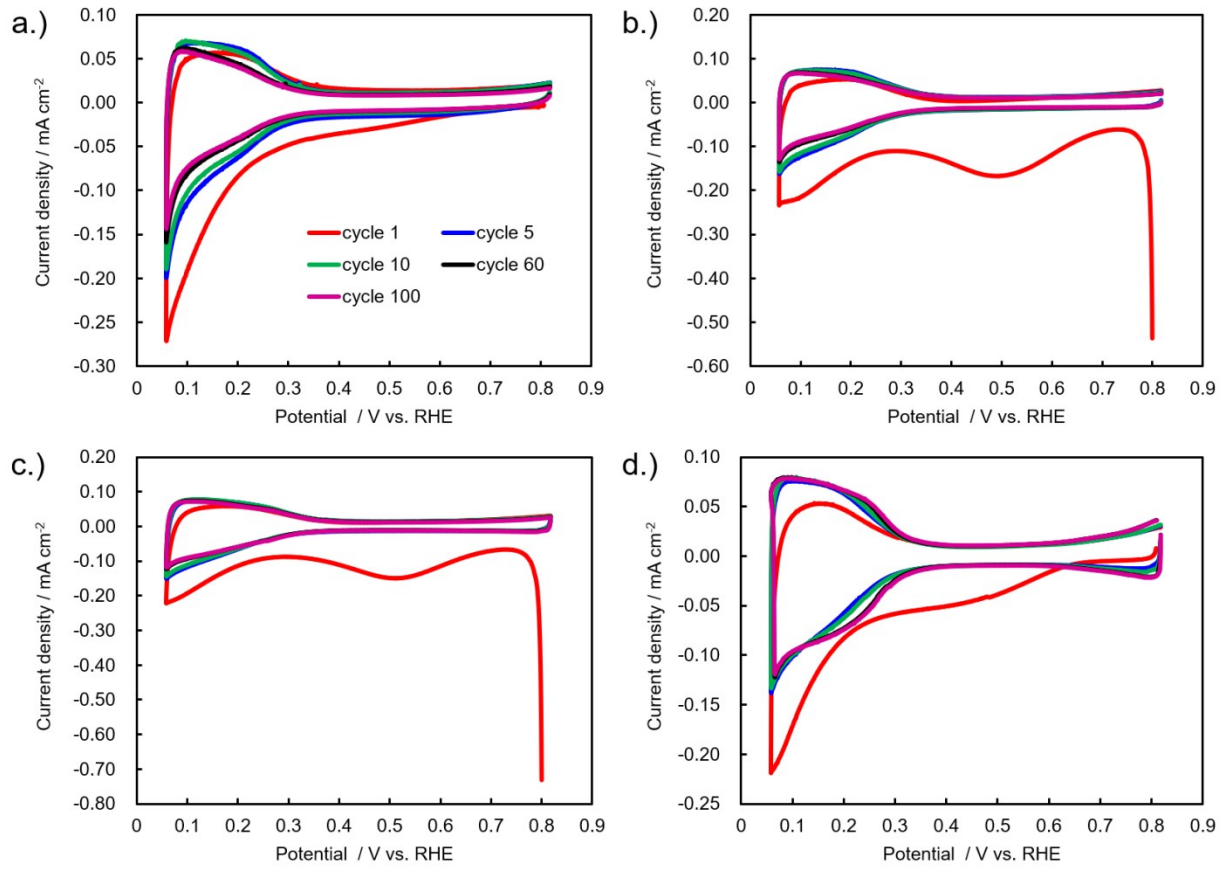

Figure S7. Narrow window CVs conducted at 100 mVs^{-1} over a range of 0.06 – 0.82 V vs. RHE in 0.5 M deaerated H_2SO_4 for SiO_x|(thin Pt) electrodes at varying cycle numbers for SiO_x thicknesses of a.) 0 nm b.) 1.6 nm c.) 4.8 nm and d.) 7.9 nm.

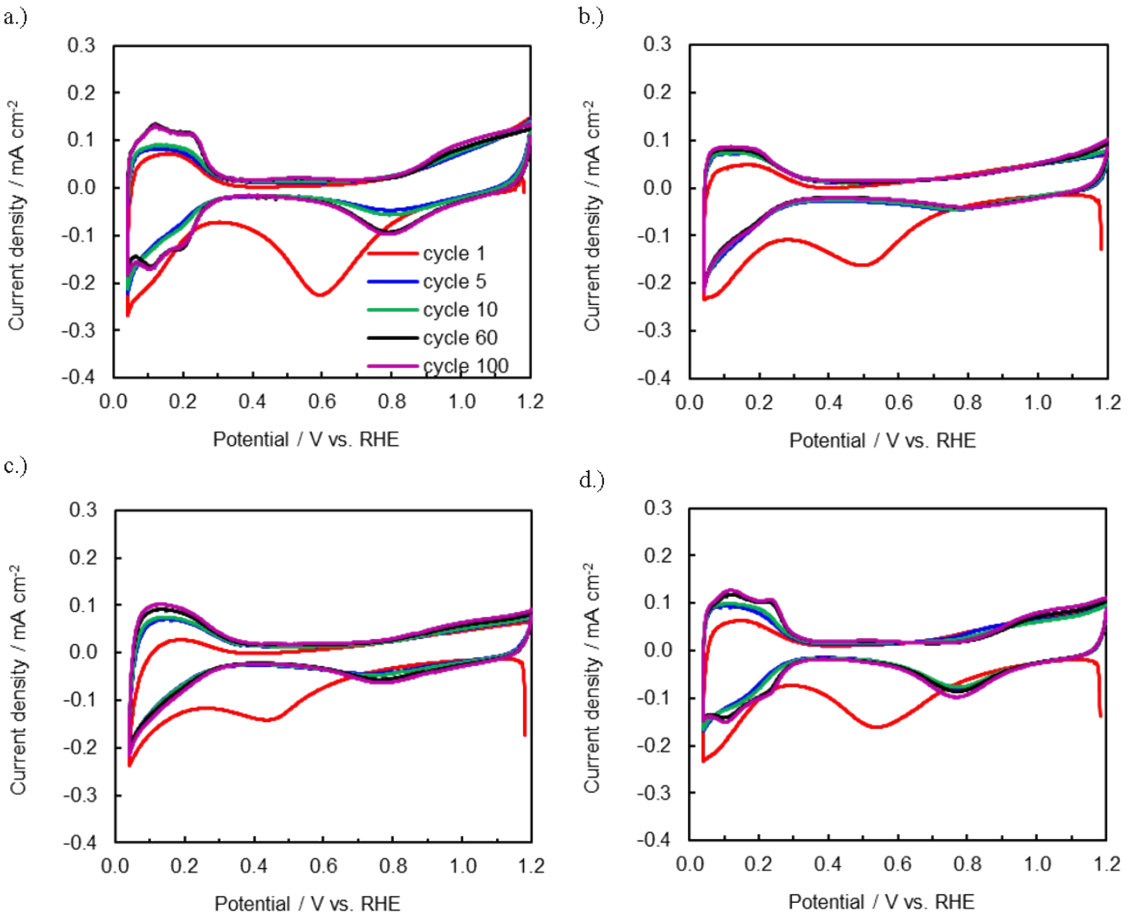

Figure S8. Wide window CVs conducted at 100 mV s^{-1} over a range of 0.06 – 1.22 V vs. RHE in 0.5 M deaerated H_2SO_4 for SiO_x|(thin Pt) electrodes at varying cycle numbers for SiOx thicknesses of a.) 0 nm b.) 1.6 nm c.) 4.8 nm and d.) 7.9 nm.

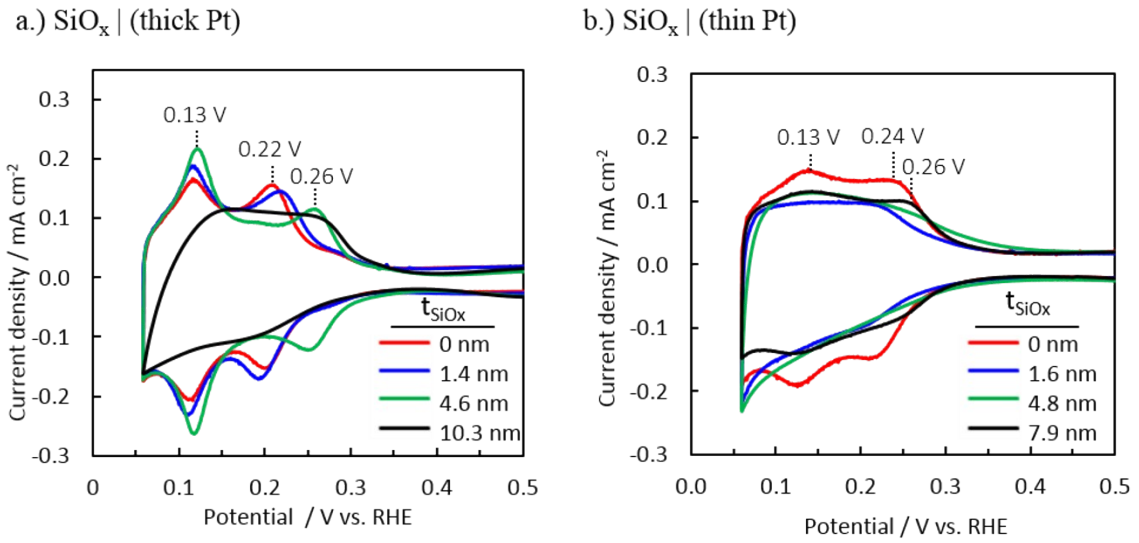

Figure S9. Zoomed-in view of H_{upd} region of wide window CVs for a.) SiO_x|(thick Pt) and b.) SiO_x|(thin Pt) electrodes, taken from main article Figures 3 and 5, respectively. CVs were measured in 0.5 M H_2SO_4 at 100 mV s^{-1}.

IV. Cu stripping voltammetry curves

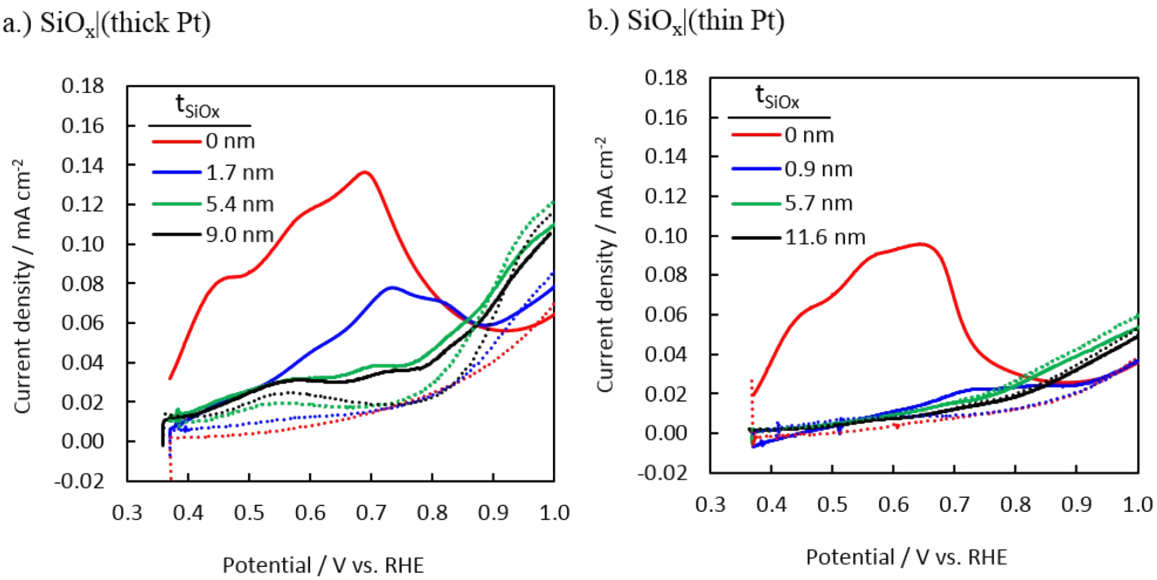

Figure S10. Cu stripping voltammetry curves (solid lines) with recorded in 2 mM $CuSO_4$ + 0.1 M H_2SO_4 with background curves (dashed lines) performed in 0.1 M H_2SO_4 for a.) SiO_x|(thick Pt) electrodes and b.) SiO_x|(thin Pt) electrodes. For all measurements, the potential of the electrode was held at +0.358 V vs. RHE for 50 seconds before sweeping the potential from +0.358 V to +1.0 V RHE at 100 mV s^{-1}.

V. Characterization of SiOx|Pt electrodes post CV cycling

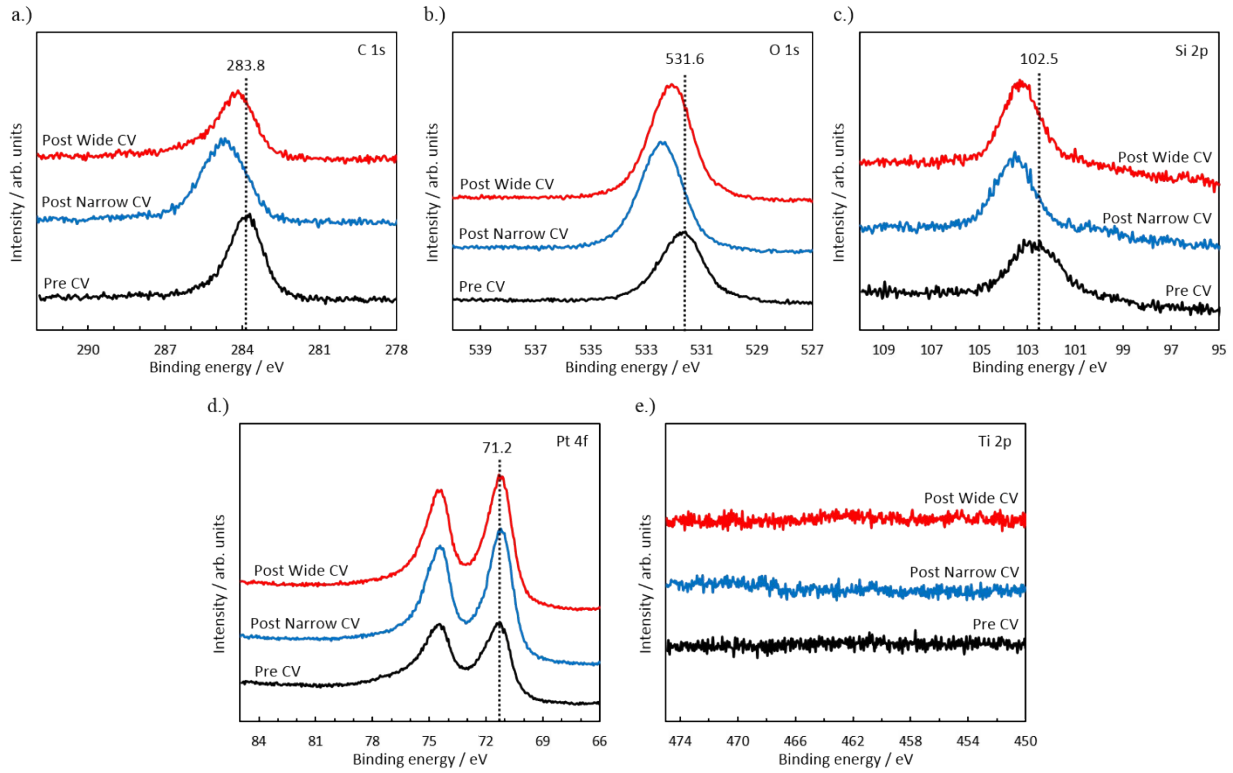

Figure S11. XPS characterization of 1.0 nm SiO_x|(thick Pt) electrodes before and after 1 hour of CV cycling in deaerated 0.5 M H_2SO_4 over narrow (0.06 V-0.82 V vs. RHE) and wide (0.06 V-1.22 V vs. RHE) potential windows. a.) Comparison of C 1s XPS spectra. b.) Comparison of O 1s XPS spectra. c.) Comparison of Silicon 2p XPS spectra. d.) Comparison of Platinum 4f XPS spectra. e.) Comparison of Ti 2p XPS spectra.

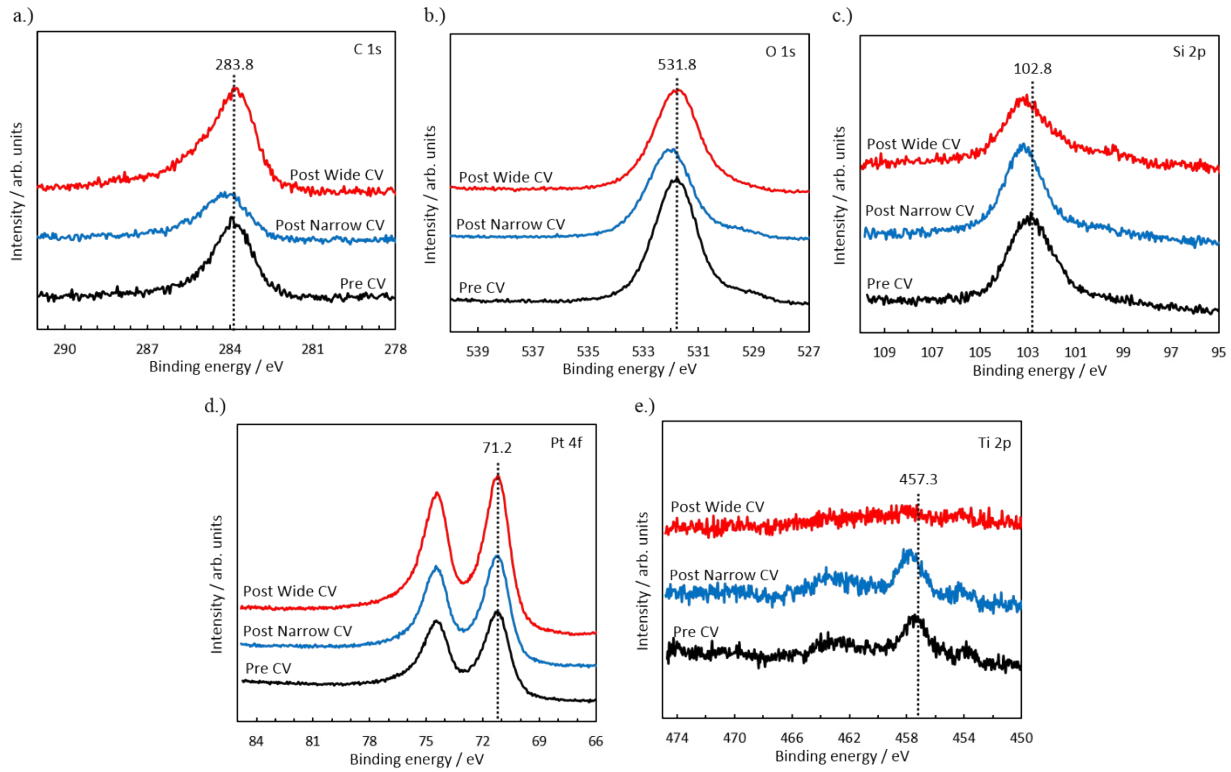

Figure S12. XPS characterization of 1.6 nm SiO_x|(thin Pt) before and after 1 hour of CV cycling in dearated 0.5 M H_2SO_4 over narrow (0.06 V-0.82 V vs. RHE) and wide (0.06 V-1.22 V vs. RHE) potential windows. a.) Comparison of C 1s XPS spectra. b.) Comparison of O 1s XPS spectra. c.) Comparison of Silicon 2p XPS spectra. d.) Comparison of Platinum 4f XPS spectra. e.) Comparison of Ti 2p XPS spectra.

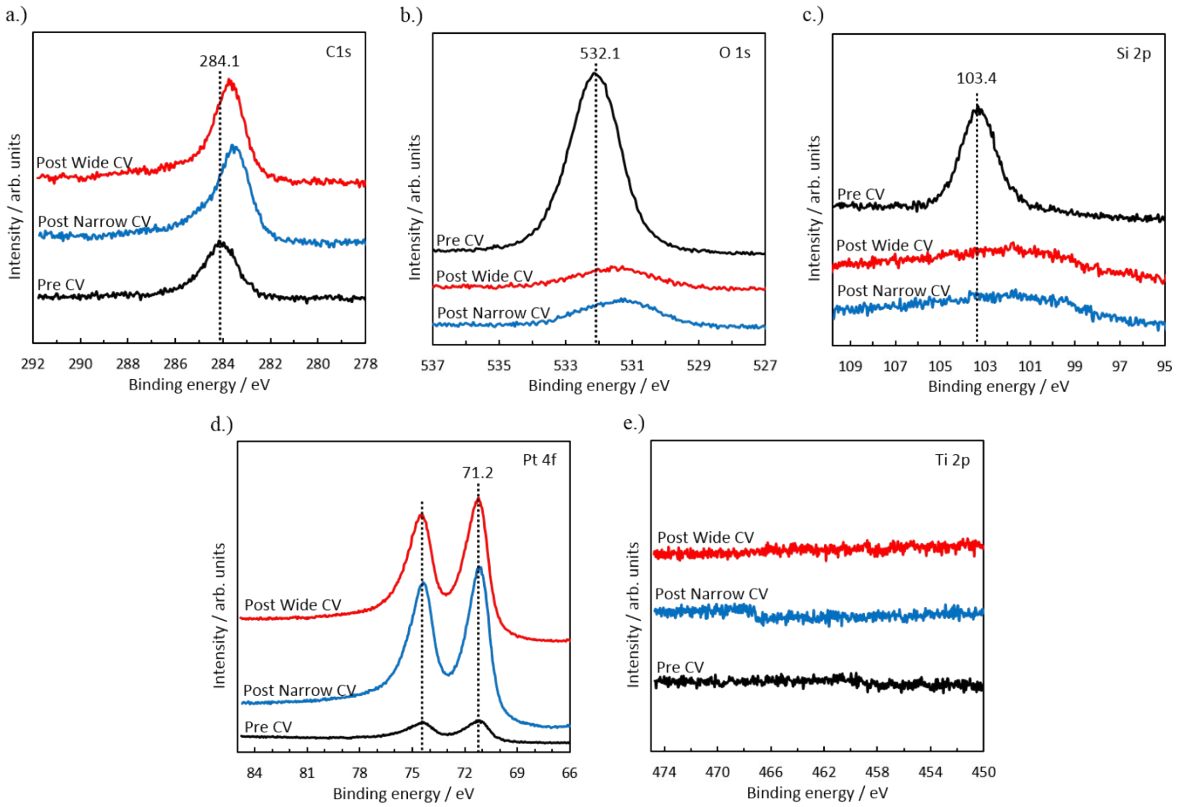

Figure S13. XPS characterization of 4.8 nm SiO_x|(thick Pt) electrodes before and after 1 hour of CV cycling in deaerated 0.5 M H_2SO_4 over narrow (0.06 V-0.82 V vs. RHE) and wide (0.06 V-1.22 V vs. RHE) potential windows. a.) Comparison of C 1s XPS spectra. b.) Comparison of O 1s XPS spectra. c.) Comparison of Silicon 2p XPS spectra. d.) Comparison of Platinum 4f XPS spectra. e.) Comparison of Ti 2p XPS spectra.

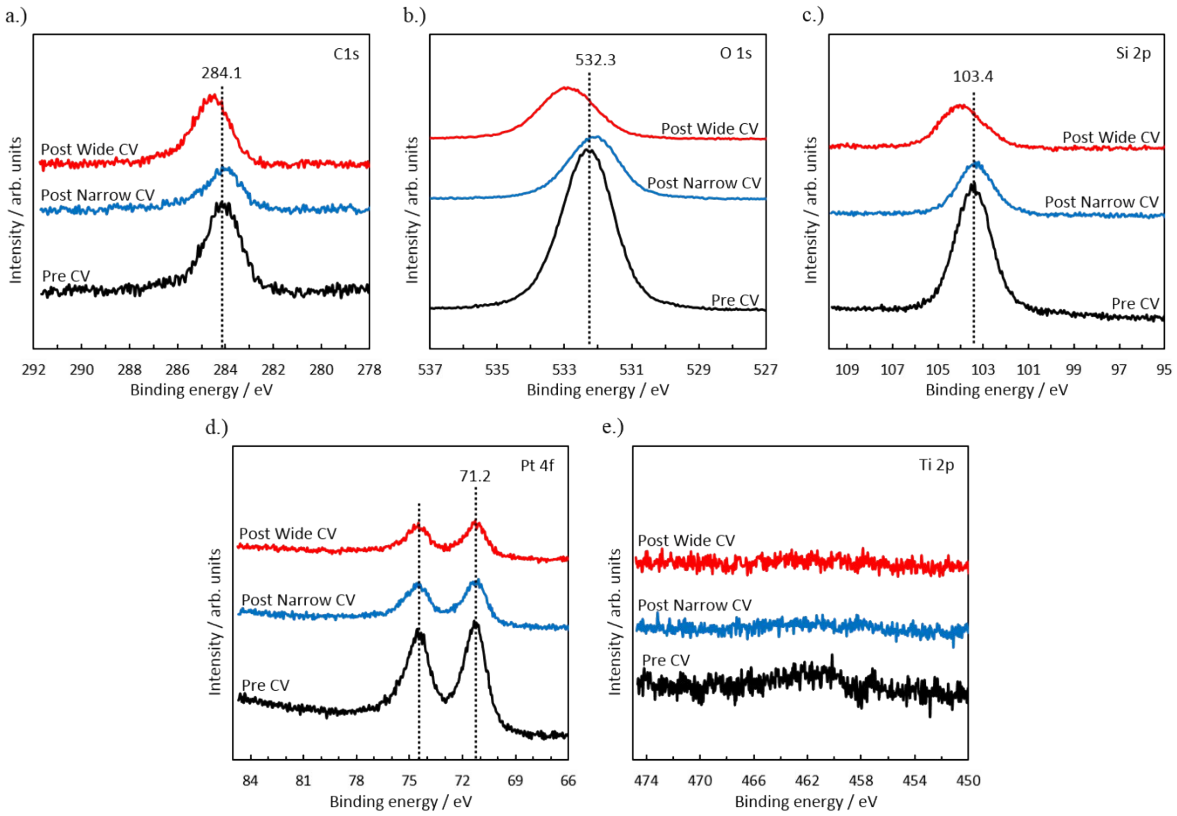

Figure S14. XPS characterization of 4.8 nm SiO_x|(thin Pt) electrodes before and after 1 hour of CV cycling in deaerated 0.5 M H_2SO_4 over narrow (0.06 V-0.82 V vs. RHE) and wide (0.06 V-1.22 V vs. RHE) potential windows. a.) Comparison of C 1s XPS spectra. b.) Comparison of O 1s XPS spectra. c.) Comparison of Silicon 2p XPS spectra. d.) Comparison of Platinum 4f XPS spectra. e.) Comparison of Ti 2p XPS spectra.

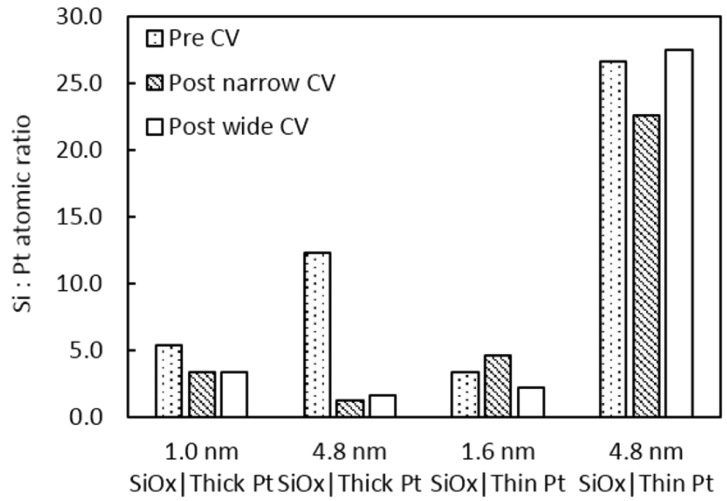

Figure S15. Comparison of the atomic Si:Pt ratio of various SiO_x thicknesses on thick and thin Pt electrodes before and after CV measurements conducted for one hour in 0.5 M H_2SO_4. Ratios were computed based on the background-subtracted peak areas of the Si 2p and Pt 4f spectra from Figures S11-S14.

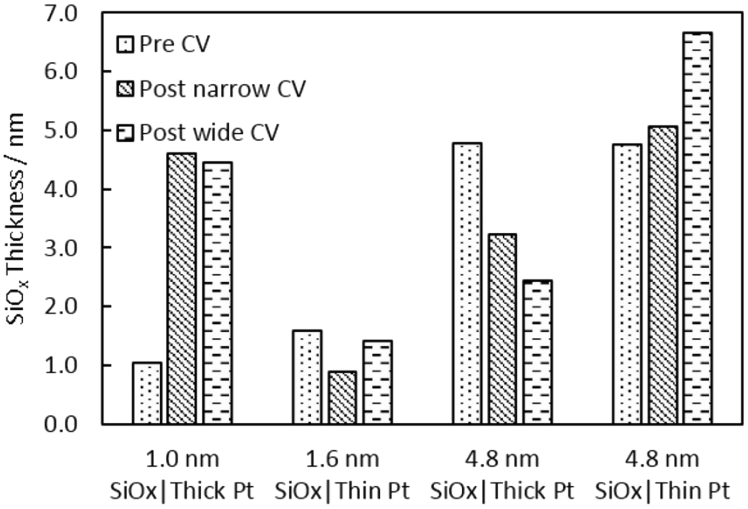

Figure S16. Comparison of apparent SiO_x thicknesses (t_{SiOx}) measured by ellipsometry before ("as-made") and after CV measurements conducted for one hour in 0.5 M H_2SO_4.

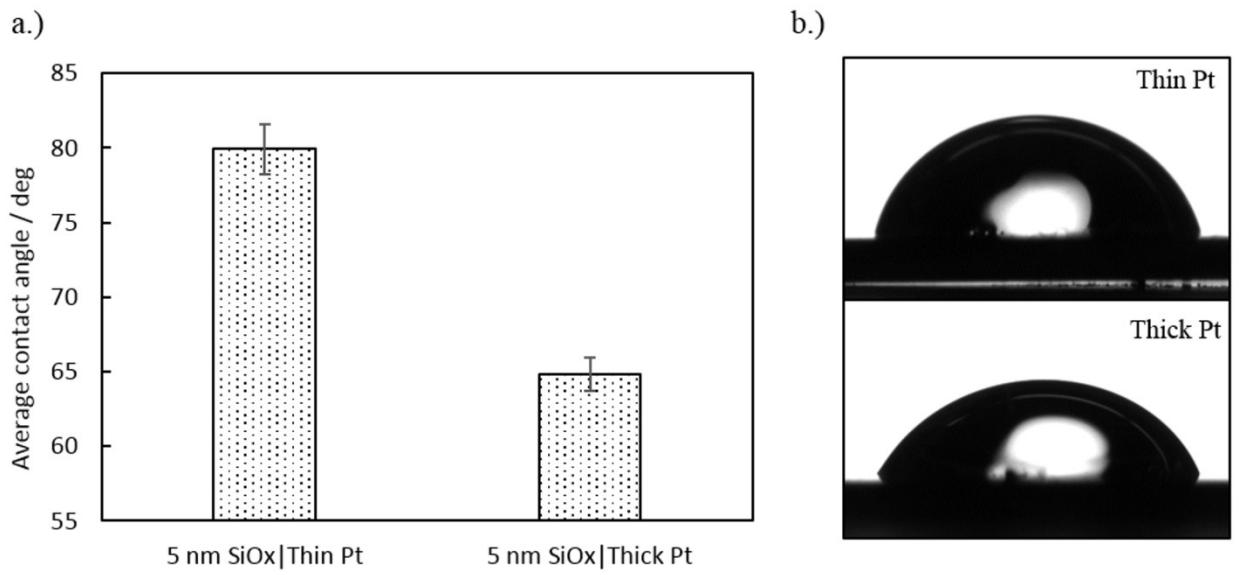

Figure S17. a.) Average contact angles measured using 10 μL of DI water for as-made overlayers on thick and thin Pt substrates. b.) Representative droplet images for samples measured in a.). The contact angle is defined as the angle between the droplet/surface interface and air/droplet interface at the triple phase boundary point. Error bars represent 95% confidence intervals for the average contact angle and were calculated from 6 measurements of 2 different samples based on a 2-sided Student's t distribution.

VI. ESI References

1 J. F. Moulder, W. F. Stickle, P. E. Sobol and K. D. Bomben, 1995, 1–261.
2 C. D. Wagner, R. H. Raymond and L. H. Gale, 1981, **3**, 211–225.
3 K. S. Kim, N. Winograd and R. E. Davis, *J. Am. Chem. Soc.*, 1971, **93**, 6296–6297.
4 M. P. Seah and W. A. Dench, *Surf. Interface Anal.*, 1979, **1**, 2–11.